Landau model for polymer-stabilized ferroelectric liquid crystals: Experiment and theory

Paul Archer,[1] Ingo Dierking,[1,*] and Mikhail Osipov[2]
[1]*School of Physics and Astronomy, University of Manchester, Schuster Laboratory, Oxford Road, Manchester M13 9PL, United Kingdom*
[2]*Department of Mathematics, University of Strathclyde, Glasgow G1 1XH, United Kingdom*
(Received 27 June 2008; published 18 November 2008)

The interaction between a phase separated polymer network and a liquid crystal was studied across the smectic-*A** (Sm-*A**) to smectic-*C** (Sm-*C**) phase transition of a polymer-stabilized ferroelectric liquid crystal polymerized in the Sm-*A** phase. Using precise measurements of the tilt angle and the spontaneous polarization as functions of the external electric field and polymer concentration, the effective coefficients of the Landau expansion of the free energy of the Sm-*C** phase have been determined experimentally. The observed polymer concentration dependence of the Landau expansion coefficients is explained using a more general theoretical model which incorporates the effect of polymer networks on the local liquid crystal director configuration. In particular, using experimental estimates of the penetration depth of the polymer network into the liquid crystal, it is shown that the *b* coefficient calculated from the Landau model increases with polymer concentration, evidencing the relationship determined experimentally.

DOI: 10.1103/PhysRevE.78.051703 PACS number(s): 61.30.Dk, 64.70.M−, 77.84.Nh

I. INTRODUCTION

Polymer-stabilized liquid crystals (PSLC) represent an exciting class of functional materials which retain the useful electro-optic properties of common liquid crystals, but also gain some unique further abilities and functionalities. The application potential of PSLC's is large and wide ranging with uses as diverse as privacy windows, reflective display devices, heat repelling sheets, and optic devices in switchable photonics and dynamic holography. Ferroelectric liquid crystals (FLC's) possess exceptional electro-optic properties with response times in the order of microseconds [1], however, their potential has not yet been fully realized due to their inherent mechanical sensitivity. The addition of a polymer network into the FLC not only increases the mechanical stability without the loss of the favorable electro-optic properties [2] but also opens up new avenues of device research such as gray scale displays via V-shaped switching [3,4] or devices which require a ground-state memory.

A thorough understanding of the interaction between liquid crystals and the stabilizing polymer network is of paramount importance for any application of these modern composite materials. The elastic coupling between the polymer network and the liquid crystal of polymer-stabilized ferroelectrics (PSFLC's) has been investigated previously. These studies have focused on the effect of the polymer network on the smectic-*A** (Sm-*A**) phase where the local effect of the polymer network on the director configuration is less significant [5], and on short pitch ferroelectric smectic-*C** (Sm-*C**) phases [6]. This work extends knowledge of the polymer network influence through the transition into the applicationally more important nonhelical surface stabilized ferroelectric Sm-*C** phase. A rigorous experimental technique involving high precision tilt angle and total polarization measurements for varying applied electric fields through the Sm-*A** to Sm-*C** transition is utilized to initially calculate the elastic coupling and the coefficients of the full Landau potential. The coefficients are then evaluated according to a Landau–de Gennes theory which takes into consideration the effect of the polymer network on the local liquid crystal director profile around the polymer strand.

Polymer-stabilized liquid crystals consist of a relatively low concentration of a photopolymerized bifunctional monomer (typically less than 10 wt. %). Prior to photopolymerization the often mesogenic monomers align themselves with the LC host, while the liquid crystal phase behavior is largely retained [7]. Under UV illumination the bifunctional monomers polymerize while phase separating from the continuous liquid crystal medium, forming a stable cross-linked fibrillike polymer network in the general direction of the liquid crystals director [8]. The network then behaves as a template of the liquid crystal order in which it was formed, aiding to align the liquid crystal [9–11]. This effect has been observed for PSLC's formed in a variety of liquid crystal phases, mainly nematic and cholesteric (*N**) phases, but also for ferroelectric liquid crystals. In the present case of a PSFLC, photopolymerized in the Sm-*A** phase, the network forms parallel to the smectic layer normal. This network generates a local elastic coupling with the liquid crystal which acts to preserve the orthogonal director configuration of the Sm-*A** phase, even on cooling into the tilted Sm-*C** phase.

II. GENERALIZED LANDAU MODEL OF THE Sm-*A** TO Sm-*C** TRANSITION

The primary scalar order parameter of the Sm-*A** to Sm-*C** phase transition is the angle between the liquid crystal director and the smectic layer normal, the tilt angle Θ [12]. In the Sm-*A** phase the director aligns parallel with the layer normal such that $\Theta=0$. On cooling into the Sm-*C** phase Θ varies to $\pm\Theta\neq 0$. This change in order parameter can either be a first order (discontinuous) or second order (continuous) transition and is well described by the general-

*ingo.dierking@manchester.ac.uk

ized Landau model of ferroelectric liquid crystals [13,14]. In a surface stabilized device subjected to an external electric field E the difference in the free energy density between the Sm-A^* and Sm-C^* phase $g-g_0$ is given by

$$g-g_0=\frac{1}{2}\alpha(T-T_C)\Theta^2+\frac{1}{4}b\Theta^4+\frac{1}{6}c\Theta^6+\frac{P^2}{2\varepsilon_0\chi_0}-C\Theta P-\frac{\Omega P^2\Theta^2}{2}-PE, \quad (1)$$

where Θ is the tilt angle, P is the total polarization, α, b, and c are the first three Landau expansion coefficients, C is the bilinear coupling coefficient, χ_0 is the high frequency dielectric susceptibility in the direction of the electric field, Ω is the biquadratic coupling coefficient, and T_C is the transition temperature of the related achiral Sm-A to Sm-C transition. The difference between the achiral Sm-A to Sm-C and the chiral Sm-A^* to Sm-C^* transition T_C^* is given by

$$T_C^*=T_C+\frac{\varepsilon_0\chi_0C^2}{\alpha}. \quad (2)$$

For low polarization systems (i.e., systems with a spontaneous polarization less than approximately 25 nC cm^{-2}) where both C and χ_0 are relatively small and α is large it is generally $T_C\approx T_C^*$. For the FLC matrix utilized in this study the difference between the two transition temperatures is 0.02 K (using the values of C, χ_0, and α obtained in Refs. [15,16]), smaller than the observable experimental resolution.

For PSFLC systems more terms are required in the generalized Landau model to take into account the interaction between the polymer network and the liquid crystal. Employing the simple model of Li *et al.* [17] the interaction between the polymer network and the liquid crystal director can be thought of as a fieldlike effect which acts to restore the local liquid crystal director to the orientation of the polymer network. The model assumes that the network is rigid, exerting a bulk anchoring force on the liquid crystal director. They introduced an elastic coupling interaction term $\frac{1}{2}W_P\sin^2\Theta\approx\frac{1}{2}W_P\Theta^2$ into the free energy density where W_P is the interaction coefficient between the polymer network and the liquid crystal director. The free energy density then reads as

$$g-g_0=\frac{1}{2}\alpha(T-T_C)\Theta^2+\frac{1}{2}W_P\Theta^2+\frac{1}{4}b\Theta^4+\frac{1}{6}c\Theta^6+\frac{P^2}{2\varepsilon_0\chi_0}-C\Theta P-\frac{\Omega P^2\Theta^2}{2}-PE. \quad (3)$$

Minimization of the free energy density [Eq. (3)] with respect to the total polarization P leads to the relation

$$P=\frac{C\Theta+E}{\frac{1}{\varepsilon_0\chi_0}-\Omega\Theta^2}, \quad (4)$$

which is equivalent to that found for neat FLC's [18,19]. Simultaneous fitting of the total polarization as a function of tilt angle with respect to varying applied electric field amplitude allows the determination of C, χ_0, and Ω. Minimization of Eq. (3) with respect to Θ and resubstitution of Eq. (4) leads to a temperature-tilt relationship of

$$T(\Theta,E)=T_C-\frac{1}{\alpha}\left[W_P+b\Theta^2+c\Theta^4-\frac{(C\Theta+E)\left(\frac{C}{\varepsilon_0\chi_0}+\Omega\Theta E\right)}{\Theta\left(\frac{1}{\varepsilon_0\chi_0}-\Omega\Theta^2\right)^2}\right]. \quad (5)$$

With the knowledge that for low polarization systems it is $T_C\approx T_C^*$ (see earlier) Eq. (5) can be directly employed to determine α, b, c, and W_P via a second set of simultaneously fitted curves $T(\Theta,E)$, using the previously determined parameters C, χ_0, and Ω.

III. EXPERIMENT

The liquid crystalline host material used in this investigation was a commercial room temperature ferroelectric mixture FELIX M4851/050 (Clariant, Germany) with phase sequence on cooling: I 73.9 °C N^*, 68.9 °C Sm-A^*, 64.4 °C Sm-C^* −20 Cry. The liquid crystal was mixed at varying concentration with a bifunctional photoreactive mesogenic diacrylate monomer RM257 (Merck). A small amount of benzoic methyl ether (2 wt. % of the monomer concentration) was added to the mixture to initiate photopolymerization. The liquid crystal–monomer mixtures were capillary filled in the isotropic phase into 5-μm-thick sandwich cells with planar alignment layers and electrode area of 25 mm^2 (AWAT PPW, Poland). The samples were then polymerized by UV irradiation of peak wavelength 352 nm and power density 0.1 mW cm^{-2} for 2 h in the Sm-A^* phase at varying monomer concentrations. The electro-optic setup included a polarizing microscope (Leica DMLP) in conjunction with a Mettler hotstage (FP82HT) and temperature controller (FP90) for relative temperature control within 0.1 K. Electric fields were applied by a function generator (Thurlby Thandar TGA12101) via an in house built fixed-gain high voltage amplifier.

For the tilt angle measurements a digital oscilloscope (Tektronix TDS3024B) was used to record the electro-optic response from an in house built photodiode. Tilt angles were determined according to a high-resolution technique introduced by Bahr and Heppke [20] using square wave applied voltages. This method allows optical tilt angle measurements with accuracies of approximately 0.1°. Polarization measurements were carried out by the well-known triangular wave method [21]. Integration of one half cycle of the reversal current after subtraction of the Ohmic current contribution results in the determination of the total polarization P. Texture images were taken with a digital camera (JVC KY-F1030) of resolution 1280×960. Scanning electron microscope (SEM) images were taken using a FEI Sirion scanning electron microscope. To allow SEM to be performed on the polymer network structures, the host liquid crystal first needs

to be removed and the polymer strands need to be metal coated. Using a technique described in Ref. [8] the samples were soaked in Hexane for several days to remove the liquid crystal from the sample cells. The samples were intermittently observed by polarising microscopy to ensure that the polymer network was undamaged by the solvent. The glass substrates were then carefully separated and dipped in hexane once more to remove any excess liquid crystal. The polymer was coated with a thin layer of gold of approximately 20 nm thickness using a metal film coating system (Edwards E306A). The software tool IMAGEJ, developed by the National Institute of Health, USA, was utilized to analyze both the optical texture and SEM images.

IV. RESULTS AND DISCUSSION

The phase transition temperatures of the liquid crystal-monomer mixtures prior to UV polymerization are depicted in Fig. 1(a) as determined by polarising microscopy on slow cooling. Addition of the monomer reduces the temperature of all the phase transitions as expected and as has also been observed previously [22]. For the materials used in this study the Sm-A^* phase vanishes for monomer concentrations above 5 wt. %, resulting in a direct N^* to Sm-C^* transition. As such only concentrations up to 4 wt. % were subjected to the UV polymerization treatment, the phase diagram of the resulting samples being displayed in Fig. 1(b). The transition temperatures approximately restore to that of the neat sample, however, the phase sequence alters for increasing polymer content, changing from $I-N^*-$Sm-A^*-Sm-C^* for the neat sample to $I-N_\infty{}^*-$Sm-A^*-Sm-C^* for the 3 and 4 wt. % PSFLC's, where $N_\infty{}^*$ denotes a chiral nematic phase with infinite pitch (for the cell gap employed in this study). This can easily be verified by texture observation, where the N^* state at low polymer concentration can not be brought to extinction by rotating the sample between crossed polarizers, while the $N_\infty{}^*$ state at higher polymer concentration can be brought to extinction.

Figure 2 displays an exemplary optical texture image of the polymer network formed by a 3 wt. % PSFLC photopolymerized in the Sm-A^* phase. The image is taken in the isotropic phase and rotated slightly out of the direction of crossed polarizers to allow visualization of the network. The bright strands observed are the polymer strands visible between crossed polarizers due to the residual birefringence of the polymer network and surrounding aligned liquid crystal molecules. The image shows a fibril-like network that forms parallel to the initial director orientation of the liquid crystal prior to polymerization, denoted here as **n**.

To examine both the size and orientation of the polymer network, SEM images were taken at a variety of magnifications and locations on a 4 wt. % polymer network. An exemplary SEM image is shown in Fig. 3 at a magnification of $\times 20\,000$, clearly evidencing a fibril-like network oriented in one general, average direction. Figure 4(a) depicts the polymer strand thickness distribution as determined by analyzing multiple SEM images of the 4 wt. % PSFLC sample. The distribution obtained is asymmetric with a peak value of 180 nm. Subtraction of the gold coating layer results in an actual average polymer strand thickness of approximately 130 nm, comparable to previously reported values [23]. The angular orientation distribution of the polymer strands is shown in Fig. 4(b). The strands are mainly oriented along an average direction with an orientational order parameter of $S=\frac{1}{2}\langle 3\cos^2\theta-1\rangle\sim 0.9$, which is equivalent to that found for smectic phases well below the transition temperature [24]. This evidences that the orientational order of the host liquid crystal is transferred onto the polymer network.

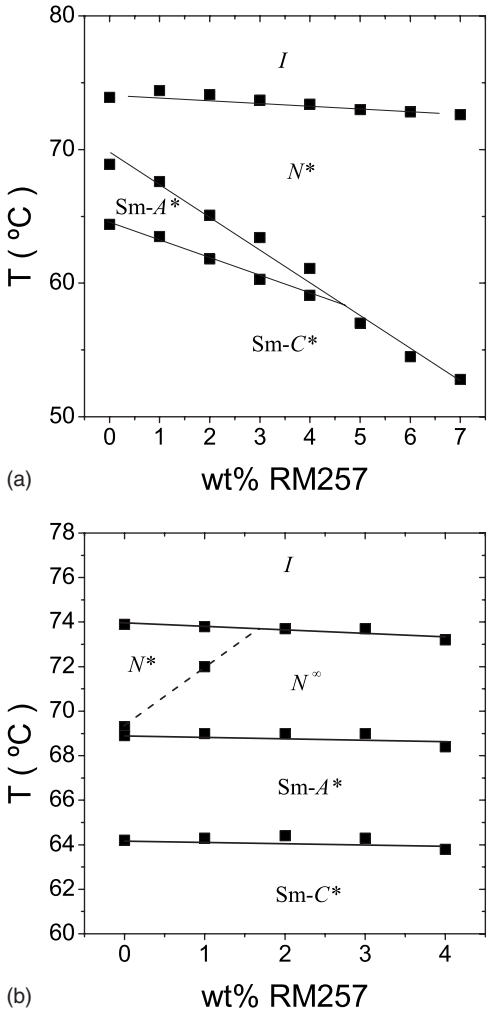

FIG. 1. Transition temperatures of the liquid crystal-polymer mixtures (a) prior to and (b) after UV polymerization in the Sm-A^* phase as determined by polarizing microscopy on slow cooling. N^* denotes a helical chiral nematic state while the notation N_∞^* refers to a chiral nematic state with infinite pitch. [The dashed line between N^* and N_∞^* in (b) is used to indicate that this does not represent a thermodynamic phase transition, but rather a structural transition from helical to nonhelical.]

The electroclinically induced tilt angle $\delta\Theta$ of all the PSFLC's studied is shown in Fig. 5 as a function of applied electric field at fixed reduced temperature in the Sm-A^* phase ($T-T_{C^*}=+1$ K). Each sample shows the expected linear response with increasing applied electric field. Additionally, we note that $\delta\Theta$ is constant for varying polymer network concentration at fixed applied field amplitudes. In the Sm-A^* phase the induced tilt angle results purely from the

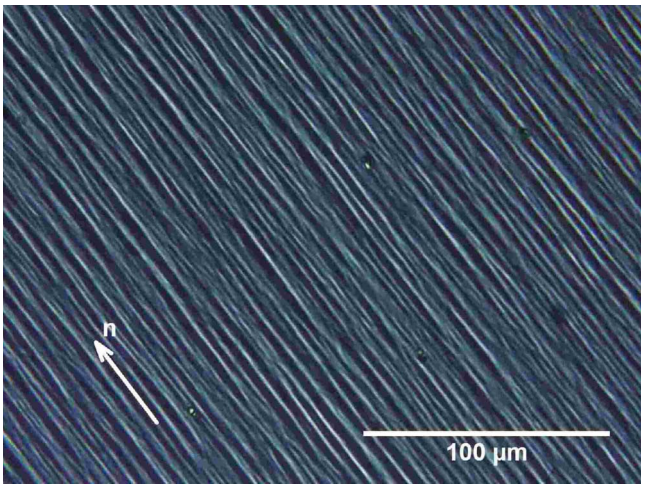

FIG. 2. (Color online) Exemplary optical microscopy image of the 3 wt. % PSFLC sample observed between crossed polarizers in the isotropic phase of the liquid crystal. The arrow denotes the director orientation of the phase in which the network was formed. The bright strands represent the polymer network, visible due to the residual birefringence of the polymer network and the surrounding liquid crystal.

electroclinic effect [25] which is inversely proportional to the first Landau coefficient α via the relation $\delta\Theta(T)=\frac{\chi_0\varepsilon_0 C}{\alpha(T-T_{C^*})}E$ [26]. The constant induced tilt angle for increasing polymer concentration leads to the conclusion that the α coefficient is also constant at the value of the neat FLC, independent of polymer concentration. Both the first Landau coefficient as well as the liquid crystal-network interaction are proportional to Θ^2 and can generally not easily be separated. But as the α coefficient has been shown to be constant for changing polymer concentration, this removes the degeneracy allowing accurate fitting of the W_P coefficient.

An example of the employed fitting procedure is shown in Fig. 6 for the 3 wt. % PSFLC sample. Figure 6(a) displays

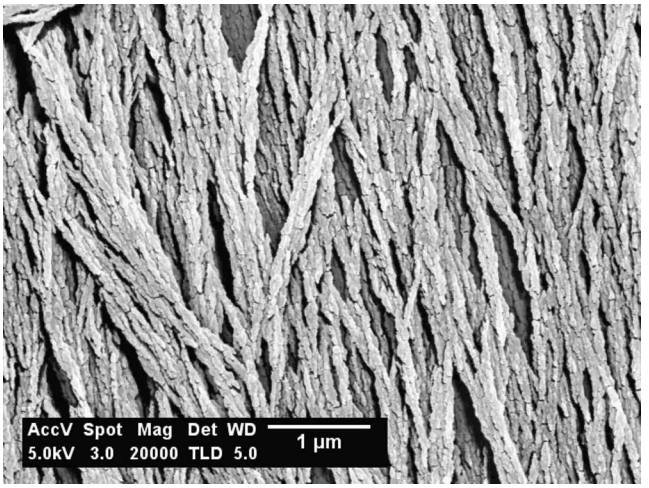

FIG. 3. Exemplary scanning electron microscopy image of the 4 wt. % PSFLC sample at ×20 000 magnification. The liquid crystal is removed and the polymer network is coated with a thin layer of gold to allow imaging.

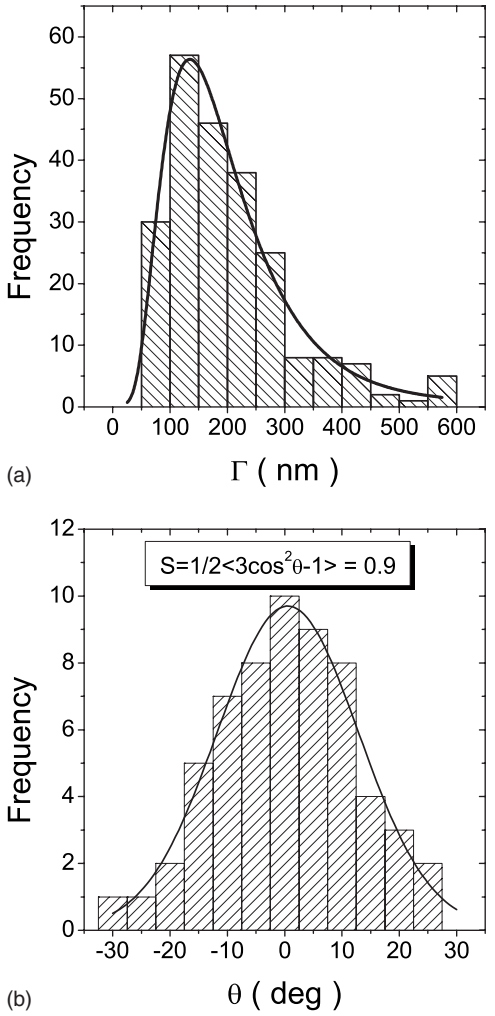

FIG. 4. (a) Distribution of the polymer strand thickness Γ as obtained by SEM of a 4 wt. % PSFLC. The peak strand thickness is approximately 130 nm (after subtraction of the gold coating). (b) Distribution of the angular orientation θ of the individual polymer strand. Analysis of the distribution results in an orientation order parameter of $S\sim 0.9$, equivalent to that found for smectic liquid crystals deep into the smectic phase.

the experimentally determined polarization P versus tilt angle Θ for varying applied electric fields with best fits (solid lines) to Eq. (4) to determine C, χ_0, and Ω. Figure 6(b) displays the experimentally determined tilt angle versus temperature for varying applied electric fields with best fits (solid lines) to Eq. (5) to determine W_P, b, and c with the α coefficient kept at the value of the neat FLC.

Figure 7 summarizes the polymer network concentration dependence of all other parameters of the generalized Landau model, b, c, C, χ_0, Ω, and W_P. As has been previously mentioned the α coefficient is assumed to be constant, taking the value of the neat FLC (α=49.5 kJ m^{-3} K^{-1} [15,16]) and hence is not shown here. Equation (4) implies that there should be no change in the polarization-tilt coupling for increasing polymer concentration. This is confirmed experimentally with no noticeable changes observed for either the C, χ_0, or Ω terms as the polymer concentration increases [Figs. 7(a)–7(c)]. The measured b coefficient, however, in-

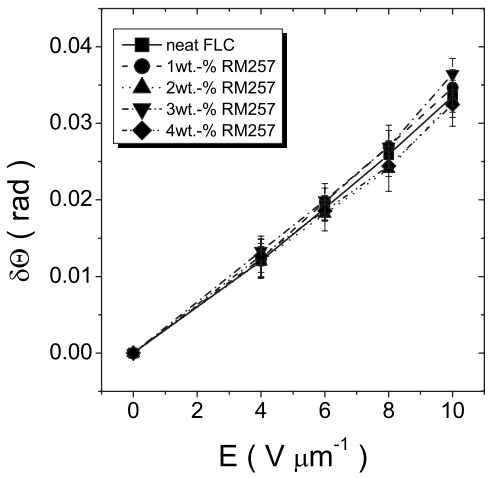

FIG. 5. Electroclinically induced tilt angle $\delta\Theta$ in the Sm-A^* phase at reduced temperature $T-T_C^*=+1$ K as a function of electric field for all polymer concentrations investigated. The constant induced tilt angle $\delta\Theta$ versus polymer concentration implies that the α coefficient does not vary with increasing polymer concentration.

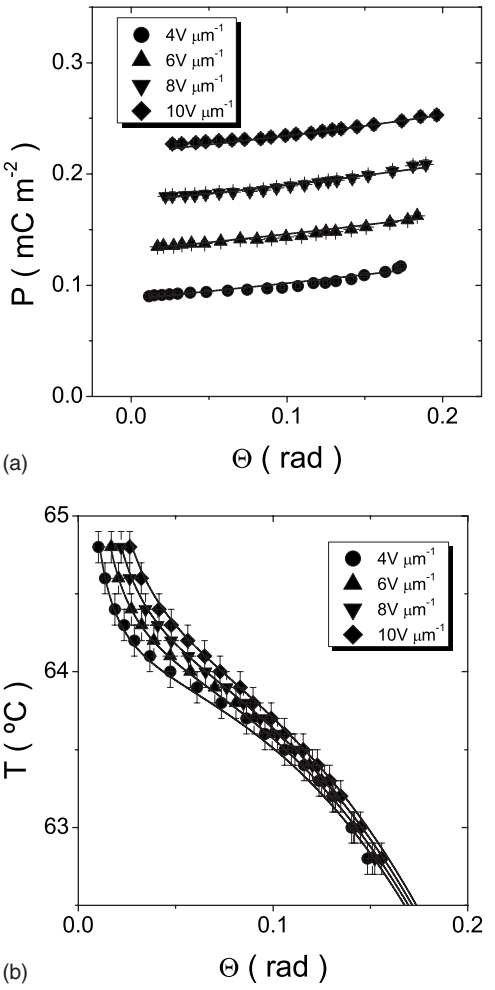

FIG. 6. Exemplary demonstration of the multicurve fitting procedure employed to determine the Landau potential. Data are shown for the 3 wt. % PSFLC sample which was polymerized in the Sm-A^* phase. (a) Experimental polarization data $P(\Theta,E)$ (symbols) and simultaneous best fits to Eq. (4) (solid lines) determine the parameters C, χ_0, and Ω. (b) Experimental tilt angle data $T(\Theta,E)$ (symbols) and simultaneous best fits to Eq. (5) (solid lines) determine W_P, b, and c with α kept at the value of the host FLC.

creases with increasing polymer content [Fig. 7(d)], the reasons of which will be discussed below. The third Landau coefficient c, Fig. 7(e), is the least well defined parameter through this experimental method as the term has its greatest influence at large tilt angles. It was observed to be approximately constant with increasing polymer concentration. The change of the elastic coupling parameter W_P between the polymer network and liquid crystal is presented in Fig. 7(f) showing an almost linear increase for increasing polymer concentration. This trend of increasing elastic interaction coefficient for increasing polymer content has been observed before [5,6,27] and will be given a thorough theoretical interpretation in terms of a more general Landau model below.

Examination of the tilt angle in the Sm-C^* phase of the PSFLC's indicates the origin of the increase of the b coefficient for increasing polymer content. Figure 8 depicts the tilt angle for selected reduced temperatures in the Sm-C^* phase for an applied electric field of 10 V μm^{-1}. For all temperatures, Θ is observed to decrease as the polymer concentration increases. Additionally, the reduction of Θ increases further away from the Sm-A^* to Sm-C^* transition. This reduction of the tilt angle of the Sm-C^* phase implies an increase in the determined b coefficient as it is observed experimentally [Fig. 7(e)]. The observed decrease in measured tilt angle may qualitatively be understood through a simple schematic diagram illustrating the local director orientation of the liquid crystal with and without a polymer strand being present (Fig. 9), and utilising the fact that the tilt angle determined experimentally is actually the average tilt angle $\langle\Theta\rangle$ of the macroscopic system. With no polymer strand present the FLC behaves as expected with $\langle\Theta\rangle=0$ in the Sm-A^* phase and $\langle\Theta\rangle=\Theta_0$ in the Sm-C^* phase. With a polymer strand present the local director orientation in the vicinity of the strand is altered such that the director aligns with the polymer strand. As the polymer network was formed in the Sm-A^* phase this results in a director orientation equivalent to that of the Sm-A^* phase, i.e., an average director parallel to the smectic layer normal. With the polymer strand present the director orientation in the Sm-A^* phase is effectively unaffected with $\langle\Theta\rangle=0$. This is not the case in the Sm-C^* phase where the tilt angle close to and far from the strand are different. Close to the strand it is $\Theta=0$, increasing to $\Theta=\Theta_0$ at some distance from it. As such, the average tilt angle of the PSFLC in the Sm-C^* phase Θ_{eff} is smaller than the tilt angle of the FLC without the polymer network present ($\langle\Theta\rangle=\Theta_{\text{eff}}<\Theta_0$). The model described in Sec. II does not take into account the effect of the polymer strand on the local director orientation around the strand and hence the tilt angle assumed is not actually the tilt angle measured experimentally.

V. EXTENDED THEORETICAL MODEL

In order to extend the current Landau model to account for this reduction of the tilt angle observed for increasing

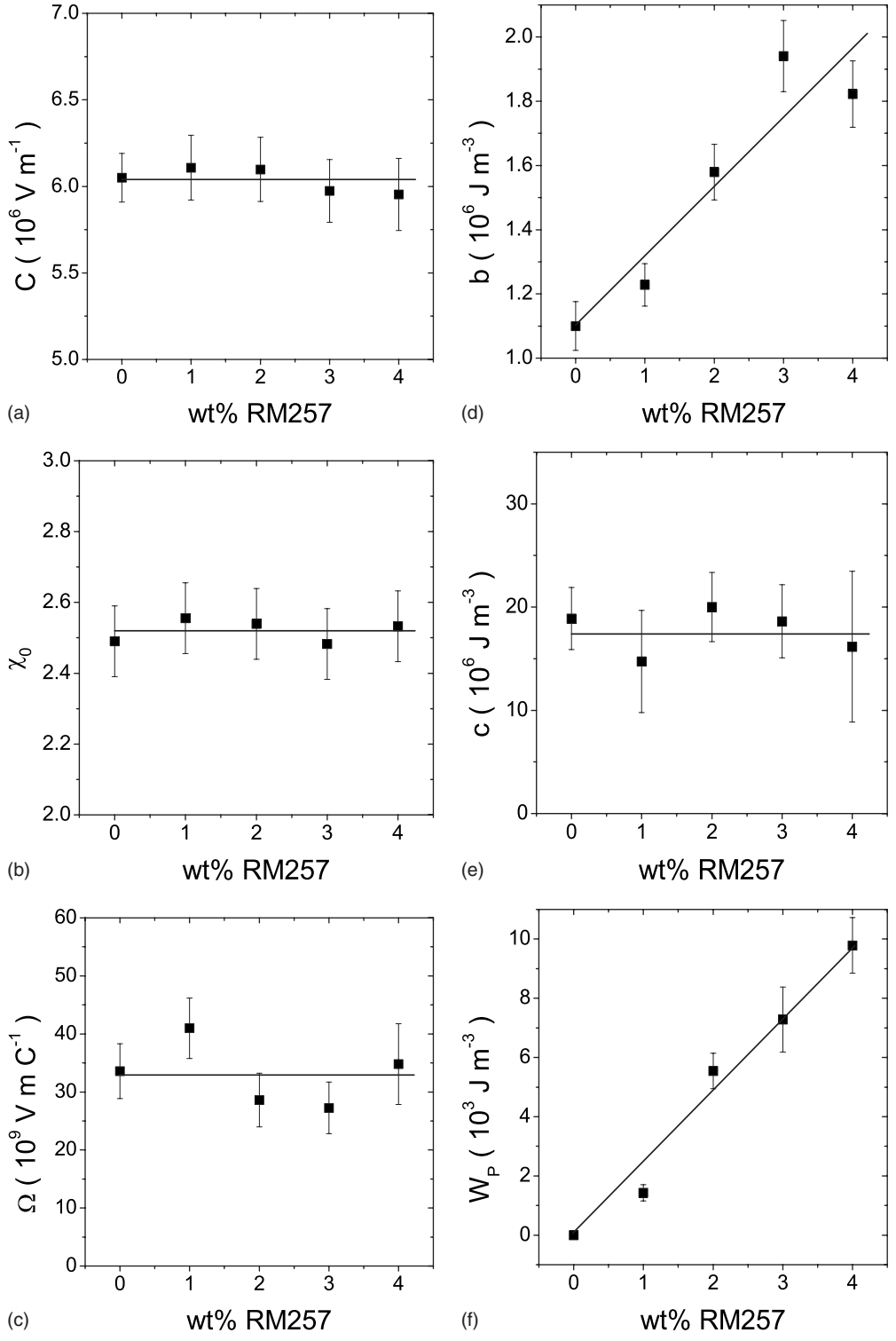

FIG. 7. Experimentally determined Landau parameters as a function of polymer concentration. (a) Bilinear polarization-tilt coupling coefficient C, (b) dielectric constant at high frequencies χ_0, (c) biquadratic polarization-tilt coupling coefficient Ω, (d) second Landau coefficient b, (e) third Landau coefficient c, and (f) elastic coupling coefficient W_P. For a detailed discussion see the text. Lines are a guide to the eye.

polymer concentration one has to take into consideration an inhomogeneous distribution of the tilt around polymer strands. This can be done in a relatively simple way making a number of assumptions. The first assumption is that the liquid crystal is strongly anchored at the surface of the polymer strand, retaining the zero tilt of the Sm-A^* phase even in the Sm-C^* phase (i.e., at the surface of the strand it is $\Theta = 0$). The tilt angle then approaches some value Θ_0 (which is the equilibrium tilt at a given temperature in the absence of the network) with an increasing distance from the strand

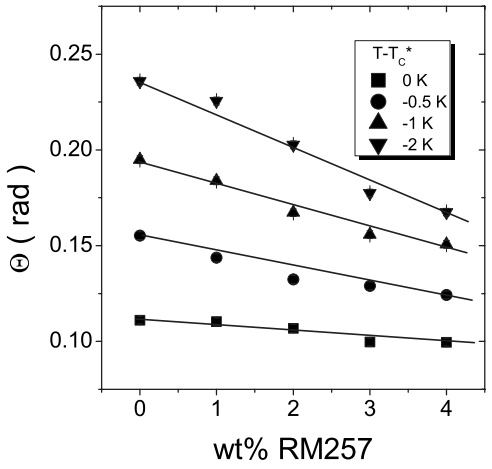

FIG. 8. Tilt angle Θ in the Sm-C^* phase at varying reduced temperatures as a function of polymer concentration for applied electric field of $E=10$ V μm^{-1}. The tilt angle decreases for increasing polymer concentration. Lines are a guide to the eye.

within a smectic layer. The expansion of the free energy density (per unit area of the smectic layer σ) in the vicinity of a strand can be written in the form

$$F/\sigma = \frac{1}{2}\alpha(T-T_C)\Theta^2 + g(\nabla\Theta)^2 + \frac{1}{4}b\Theta^4 + \frac{1}{6}c\Theta^6 + \cdots , \tag{6}$$

where the second (gradient) term describes the distortion energy determined by the inhomogeneous distribution of the tilt.

The spatially inhomogeneous distribution of the tilt angle of the smectic layer around the strand $\Theta(\mathbf{r}_\perp)$ can be determined by minimization of Eq. (6) using the boundary conditions $\Theta(0)=0$ and $\Theta\ (\mathbf{r}_\perp\to\infty)=\Theta_0$. In the general case this distribution can only be determined numerically for given values of the coefficients in Eq. (1). For a qualitative comparison with the experiment we will use a simple Ansatz distribution $\Theta(r)=\Theta_0[1-\exp(-r_i)/\lambda]$, where λ is the characteristic penetration length and r_i is the distance from the strand "i."

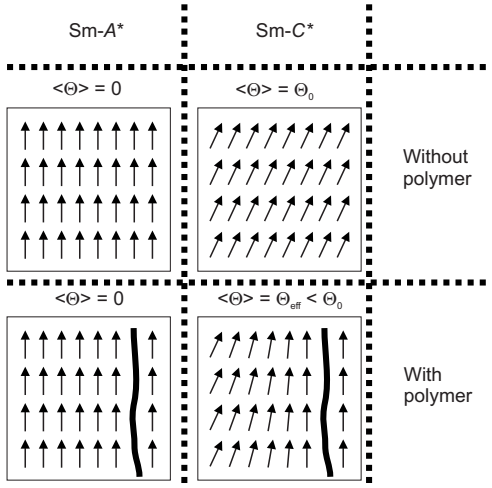

FIG. 9. Schematic diagram illustrating the director profile of the liquid crystal in both the Sm-A^* and Sm-C^* phases with and without a polymer strand present.

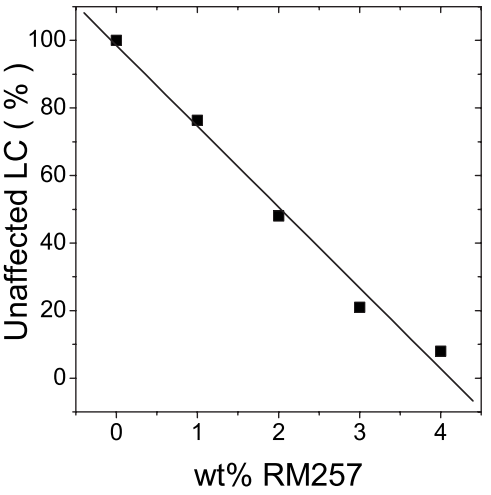

FIG. 10. Percentage of PSFLC which is unaffected by the polymer network. Data are taken by thresholding the optical images taken in the isotropic phase. The figure demonstrates that above 4 wt. % the entire cell is affected by the polymer network.

The second assumption made is that the concentration of strands is sufficiently small, so that the areas of reduced tilt around the strands practically do not intersect. In this case the distribution of the tilt angle in the smectic layer with many strands can approximately be expressed as

$$\Theta(r) = \Theta_0\left[1 - \sum_i \exp(r_i/\lambda)\right], \tag{7}$$

where $r_i=|\mathbf{r}-\mathbf{r}_i^0|$ and where $\mathbf{r}_i^0$ is the position of strand i. Experimentally it is found that the areas affected by the polymer network do not intersect for polymer concentrations of approximately 4 wt. % and below, as demonstrated by the vanishing isotropic texture appearance of Fig. 10 above 4 wt. % of polymer content.

One notes that the experimentally determined tilt angle $\tilde{\Theta}$ does not coincide with either Θ_0 or $\Theta(r)$. In an experiment an average effective (macroscopic) tilt angle is measured. Taking into account that the experimentally determined elastic coupling quantities are quadratic in Θ, the experimental tilt angle can be approximately defined as

$$\tilde{\Theta}^2 = \frac{1}{\sigma}\int \Theta^2(\mathbf{r})d^2\mathbf{r}, \tag{8}$$

where σ is the total area of the layer. Substituting Eq. (7) one obtains a relationship between the experimental tilt angle $\tilde{\Theta}$ and Θ_0:

$$\tilde{\Theta}^2 = \frac{{\Theta_0}^2}{\sigma} \int \left[1 - \sum_i \exp(-r_i/\lambda) \right]^2 r dr \approx {\Theta_0}^2 \left(1 - \frac{7}{4}\rho\lambda^2 \right), \tag{9}$$

where ρ is the surface number density of polymer strands. In the derivation of Eq. (9) we have again taken into account that the areas of modified tilt around different strands do not intersect, which implies that $\exp(-r_i/\lambda)\exp(-r_j/\lambda) \approx 0$ for $i \neq j$.

In the same way one can also obtain an expressions for the surface averages of $\Theta^4(\mathbf{r})$ and $[\nabla\Theta(\mathbf{r})]^2$ which enter the free energy density [Eq. (6)]:

$$\frac{1}{\sigma} \int \Theta^4(\mathbf{r}) d^2\mathbf{r} \approx {\Theta_0}^4 \left(1 - \frac{45}{16}\rho\lambda^2 \right), \tag{10}$$

$$\frac{1}{\sigma} \int [\nabla\Theta(\mathbf{r})]^2 d^2\mathbf{r} \approx \frac{\rho {\Theta_0}^2}{4}. \tag{11}$$

In the previous section we have analyzed the experimental data using the generalized Landau–de Gennes expansion of the total free energy in terms of the experimentally determined tilt angle. This procedure enables one to determine the coefficients of the expansion as a function of polymer concentration. The corresponding free energy expansion can also be derived using the present theoretical model. Indeed, the total free energy of the smectic layer can be obtained by surface integration of the free energy [Eq. (6)]

$$F = \int F(\mathbf{r}) d^2\mathbf{r}, \tag{12}$$

where $F(\mathbf{r})$ is given by Eq. (6). Substituting Eq. (6) into Eq. (12) and integrating over $\mathbf{r}$ using Eqs. (9)–(11) one obtains the expansion of the free energy in powers of the tilt angle Θ_0:

$$F = \frac{1}{2}\alpha(T - T_C){\Theta_0}^2 \left(1 - \frac{7}{4}\rho\lambda^2 \right) + \frac{1}{4} g \rho {\Theta_0}^2 + \frac{1}{4} b {\Theta_0}^4 \left(1 - \frac{45}{16}\rho\lambda^2 \right) + \cdots . \tag{13}$$

Using the relationship between the tilt angle Θ_0 and the experimental tilt angle $\tilde{\Theta}$ [Eq. (9)] one obtains the free energy expansion in terms of $\tilde{\Theta}$ which can directly be compared with the experiment:

$$F = \frac{1}{2}\alpha(T - T_C)\tilde{\Theta}^2 + \frac{1}{4} g \left(\frac{\rho}{1 - \frac{7}{4}\rho\lambda^2} \right) \tilde{\Theta}^2 + \frac{1}{4} b \left(\frac{1 - \frac{45}{16}\rho\lambda^2}{\left(1 - \frac{7}{4}\rho\lambda^2 \right)^2} \right) \tilde{\Theta}^4 + \cdots . \tag{14}$$

It can readily be seen that in the framework of the present model the influence of the polymer strands results in the additional quadratic term of the type $w_4(\rho)\tilde{\Theta}^2$ equivalent to the elastic interaction coefficient W_P introduced earlier with

$$W_P = w_4(\rho) = \frac{1}{4} g \left(\frac{\rho}{1 - \frac{7}{4}\rho\lambda^2} \right), \tag{15}$$

which shifts the transition temperature. According to Eq. (15) the coefficient W_P should be approximately proportional to the polymer concentration ρ for small concentrations as observed experimentally [Fig. 7(f)]. In the framework of this model the inhomogeneous distribution of the tilt also results in a renormalization of the effective expansion coefficient b which now depends on polymer concentration

$$b(\rho) = \frac{1}{4} b \frac{1 - \frac{45}{16}\rho\lambda^2}{\left(1 - \frac{7}{4}\rho\lambda^2 \right)^2}. \tag{16}$$

The coefficient b has a more complex behavior than W_P, but for small polymer concentrations b is approximately proportional to $(1 + \frac{11}{16}\rho\lambda^2)$, i.e., it increases with increasing polymer

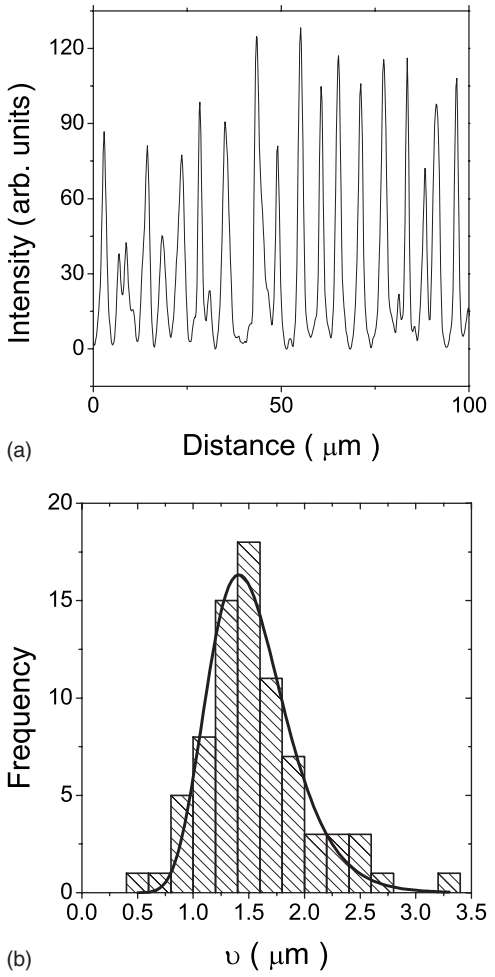

FIG. 11. (a) Exemplary intensity profile of an optical texture of the 2 wt. % PSFLC. (b) Distribution of the optically perceived strand thickness υ for the 2 wt. % RM257 PSFLC displaying an average value of 1.5 μm.

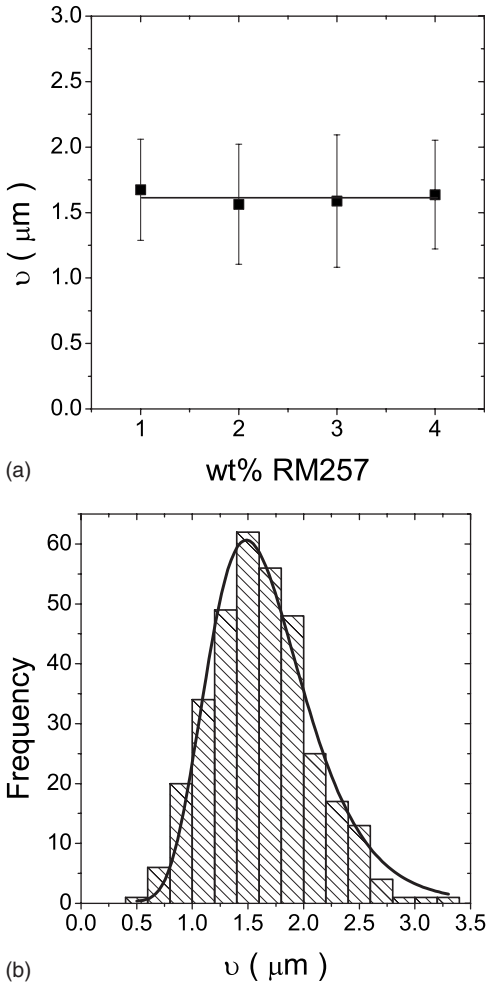

FIG. 12. (a) Average optically perceived polymer strand thickness υ versus polymer content. The invariance of υ for increasing polymer content implies that the penetration depth does not depend on the polymer network concentration. The line is a guide to the eye. (b) Distribution of all the perceived strand thicknesses υ determined irrespective of polymer concentration. The average perceived polymer strand thickness is 1.6 μm equating to a penetration depth of 750 nm.

density as observed experimentally [Fig. 7(d)]. We do not attempt to evaluate the c coefficient because the present model is too oversimplified to account for higher order terms in the expansion.

Information about the surface density of the polymer network ρ and the penetration depth of the polymer strands λ is required to fully connect the above model to the experimentally determined parameters. Making the reasonable assumption that the monomer and the liquid crystal possess the same density, ρ can be calculated by using the knowledge obtained about the average strand thickness: $\rho = W/\pi\Gamma^2$, where W is the weight fraction and Γ is the average polymer strand thickness (see Fig. 4). The value of the penetration depth can be estimated by combining information from optical microscopy and SEM images. In the isotropic phase of the PSFLC, the effect of the polymer network on the liquid crystal host is easily verified by optical microscopy (Fig. 2). Bright strands are observed due to the residual birefringence of the polymer

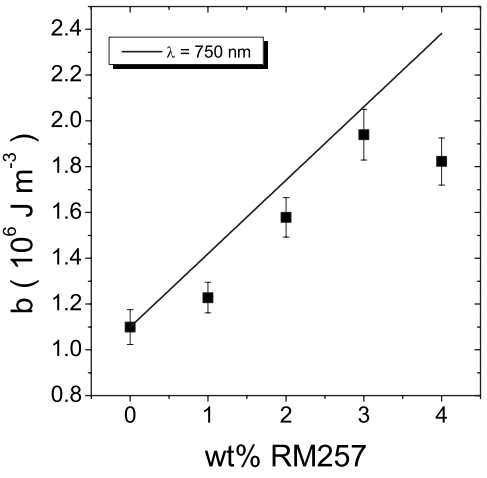

FIG. 13. Experimental b coefficient (symbols) compared to the b coefficient determined from the modified theory using the estimated penetration depth of $\lambda = 750$ nm (solid line).

network and surrounding aligned liquid crystal molecules. If the assumption is made that the anchoring strength of the liquid crystal on the polymer strand is the same for the Sm-A^* and Sm-C^* phases as it is in the isotropic phase, then subtraction of the actual strand thickness Γ from the strand thickness perceived optically υ allows an estimate of the penetration depth λ. The perceived strand thickness can be determined by taking intensity slices through the optical texture images perpendicular to the strands. One such slice is shown in Fig. 11(a) for the 2 wt. % PSFLC sample showing clearly defined peaks. Figure 11(b) shows the determined distribution of υ for the 2 wt. % samples, which was obtained by taking three intensity slices of two different texture images. Similar to the polymer strand thickness measured from SEM images (Fig. 4) the distribution is asymmetric with a peak value of about 1.5 μm. Figure 12(a) shows the average perceived strand thickness obtained as a function of concentration. It can be seen that for the concentrations employed υ is approximately constant with changing polymer content and hence the concentration has no influence on the penetration depth of the polymer network. Plotting a distribution of all the perceived strand thicknesses obtained optically [Fig. 12(b)], irrespective of concentration, results in an asymmetric distribution with a peak at 1.6 μm. Subtraction of the actual strand thickness from SEM results in an estimated penetration depth of $\lambda = 750$ nm.

With knowledge of both the polymer strand surface density ρ and the penetration depth λ, it is possible to compare the experimentally obtained b coefficient to that calculated from the above model. Figure 13 displays the determined b coefficient (symbols) as well as the calculated b coefficient (solid line) using the estimated penetration depth of 750 nm. The trend of increasing b coefficient with increasing polymer concentration is seen in both the experimentally determined and calculated b coefficients.

VI. CONCLUSIONS

The present study employed a thorough experimental technique to determine all the terms of the generalized Lan-

dau model extended to incorporate the effect of the polymer network of a polymer-stabilized ferroelectric liquid crystal (PSFLC). It was shown that the polarization-tilt coupling parameters C, χ_0, and Ω are invariant to increasing polymer concentration. At the same time the elastic coupling between the polymer network and liquid crystal director W_P increases linearly with increasing polymer concentration. The expansion coefficient b (in the fourth order term) also increases with the increasing concentration which is directly related to the decrease of the experimentally observed average tilt angle. The observed increase of these coefficients is explained using the generalized Landau–de Gennes model which accounts for the inhomogeneous distribution of the tilt around polymer strands. The local director profile in the vicinity of the polymer strands leads to the reduction of the measured tilt angle. We thus qualitatively and quantitatively characterize the influence of a phase separated polymer network on the properties of a ferroelectric liquid crystal. The generalized Landau–de Gennes potential incorporating an elastic coupling term between network and liquid crystal, as well as accounting for the director profile in the vicinity of polymer strands, is in excellent agreement with experimentally observed behavior.

ACKNOWLEDGMENTS

This work was financially supported by the EPSRC under Grant No. EP/D079128/1. Rainer Wingen of Clariant, Wiesbaden, is acknowledged for providing the ferroelectric liquid crystal host mixture FELIX M4851/050. We would like to thank Irina Grigorieva for the scanning electron microscopy images and Paul Brimicombe for valuable discussions.

[1] N. A. Clark and S. T. Lagerwall, Appl. Phys. Lett. **36**, 899 (1980); N. A. Clark, M. A. Handschy, and S. T. Lagerwall, Mol. Cryst. Liq. Cryst. **94**, 213 (1983); N. A. Clark and S. T. Lagerwall, Ferroelectrics **59**, 25 (1984).
[2] R. A. M. Hikmet, H. M. J. Boots, and M. Michielsen, Liq. Cryst. **19**, 65 (1995).
[3] Y. Miyazaki, H. Furue, T. Takahashi, M. Shikada, and S. Kobayashi, Mol. Cryst. Liq. Cryst. **364**, 491 (2001).
[4] H. Furue, T. Miyama, Y. Iimura, H. Hasebe, H. Takatsu, and S. Kobayashi, Jpn. J. Appl. Phys., Part 1 **36**, L1517 (1997).
[5] M. Petit, A. Daoudi, M. Ismaili, and J. M. Buisine, Phys. Rev. E **74**, 061707 (2006).
[6] M. Petit, A. Daoudi, M. Ismaili, and J. M. Buisine, Eur. Phys. J. E **20**, 327 (2006).
[7] I. Dierking, Adv. Mater. (Weinheim, Ger.) **12**, 167 (2000).
[8] Y. K. Fung, D.-K. Yang, S. Ling, L.-C. Chien, S. Zumer, and J. W. Doane, Liq. Cryst. **19**, 797 (1995).
[9] R. A. M. Hikmet and H. M. J. Boots, Phys. Rev. E **51**, 5824 (1995).
[10] R. A. M. Hikmet, Liq. Cryst. **9**, 405 (1991).
[11] G. A. Held, L. L. Kosbar, I. Dierking, A. C. Lowe, G. Grinstein, V. Lee, and R. D. Miller, Phys. Rev. Lett. **79**, 3443 (1997).
[12] I. Muševič, R. Blinc, and B. Žekš, *The Physics of Ferroelectric and Antiferroelectric Liquid Crystals* (World Scientific, Singapore, 2000).
[13] B. Žekš, Mol. Cryst. Liq. Cryst. **114**, 259 (1984).
[14] T. Carlsson, B. Žekš, A. Levstik, C. Filipic, I. Levstik, and R. Blinc, Phys. Rev. A **36**, 1484 (1987).
[15] P. Archer and I. Dierking, Eur. Phys. J. E **18**, 373 (2005).
[16] P. Archer and I. Dierking, Phys. Rev. E **72**, 041713 (2005).
[17] J. Li, X. Zhu, L. Xuan, and X. Huang, Ferroelectrics **277**, 85 (2002).
[18] F. Giesselmann, and P. Zugenmaier, Phys. Rev. E **52**, 1762 (1995).
[19] F. Giesselmann, A. Heimann, and P. Zugenmaier, Ferroelectrics **200**, 237 (1997).
[20] C. Bahr and G. Heppke, Liq. Cryst. **2**, 825 (1987).
[21] K. Miyasato, S. Abe, H. Takezoe, A. Fukuda, and E. Kuze, Jpn. J. Appl. Phys., Part 2 **22**, L661 (1983).
[22] H. Furue, K. Ikeda, and Y. Yamazaki, Jpn. J. Appl. Phys., Part 1 **46**, 7132 (2007).
[23] I. Dierking, L. L. Kosbar, A. Afzali-Ardakani, A. C. Lowe, and G. A. Held, Appl. Phys. Lett. **71**, 2454 (1997).
[24] A. Hauser, G. Pelzl, C. Selbmann, D. Demus, S. Grande, and A. Petrov, Mol. Cryst. Liq. Cryst. **91**, 97 (1983).
[25] S. Garoff and R. B. Meyer, Phys. Rev. Lett. **38**, 848 (1977); Phys. Rev. A **19**, 338 (1979).
[26] S. T. Lagerwall, *Ferroelectic and Antiferroelectric Liquid Crystals* (Wiley-VCH, Weinheim, 1999).
[27] I. Dierking, M. A. Osipov, and S. T. Lagerwall, Eur. Phys. J. E **2**, 303 (2000).